First-principles investigations of the structure and stability of oxygen adsorption and surface oxide formation at Au(111)

Hongqing Shi and Catherine Stampfl

School of Physics, The University of Sydney, Sydney, New South Wales 2006, Australia
(Received 18 March 2007; revised manuscript received 11 July 2007; published 15 August 2007)

We perform density-functional theory calculations to investigate the adsorption of oxygen at the Au(111) surface, including on-surface, subsurface, and surface oxide formation. We find that atomic oxygen adsorbs weakly on the surface and is barely stable with respect to molecular oxygen, while pure subsurface adsorption is only metastable. Interestingly, however, we find that the most favorable structure investigated involves a thin surface-oxide-like configuration, where the oxygen atoms are quasithreefold-coordinated to gold atoms, and the gold atoms of the surface layer are twofold, linearly coordinated to oxygen atoms. By including the effect of temperature and oxygen pressure through the description of *ab initio* atomistic thermodynamics, we find that this configuration is the most stable for realistic catalytic temperatures and pressures, e.g., for low-temperature oxidation reactions, and is predicted to be stable up to temperatures of around 420 K at atmospheric pressure. This gives support to the notion that oxidized Au, or surface-oxide-like regions, could play a role in the behavior of oxide-supported nanogold catalysts.

I. INTRODUCTION

Gold has long been regarded as catalytically inert.[1] However, since the evidence provided by Haruta *et al.* of a high catalytic activity for low-temperature CO oxidation, it has been shown that gold is active for a number of other reactions when stabilized in the form of nanoparticles on (reducible) metal oxides.[1–3] These findings have stimulated huge efforts in an attempt to understand the mechanisms responsible for the high activity, including investigations into the nature of adsorption of oxygen on gold surfaces.[4] Nevertheless, there are still many fundamental aspects that are unclear: For example, some studies of CO oxidation on TiO_2-supported gold catalysts at very low temperatures (90 K) report that the active species is the oxygen molecule,[5,6] while recent experiments find that it is atomic oxygen which reacts with CO in the temperature range of 65–250 K.[7,8] Effectively low-coordinated surface Au atoms, which are more prevalent in small Au nanoparticles, have been proposed to play a crucial role, e.g., by enhancing the dissociation of molecular oxygen or by strengthening the binding of the reactants.[9–11] Also, the altered electronic properties of gold atoms due to interaction with the oxide support,[12–14] and the effect of strain,[11] have been proposed as playing a role in the reactivity.[15]

Despite considerable efforts, even the relatively "simple" O/Au system is still not well understood on a microscopic level. With respect to the (111) surface, which we focus on in the present paper, early studies were often contradictory; Chesters and Somorjai[16] investigated the dissociative chemisorption of molecular oxygen on Au(111) and stepped Au surfaces and found that oxide formation occurs rapidly above 500 °C (773 K). The oxide was reported to be stable on both surfaces to 800 °C (1073 K) in vacuum. The presence of steps did not appear to influence this behavior. Schrader,[17] however, subsequently showed that surface-segregated calcium (a common impurity in Au samples) significantly enhances the dissociative chemisorption of oxygen at 600 °C (873 K) and it (or Si impurities[18]) may have played a role

in the former results. Legaré *et al.*[19] studied the interaction of O_2 with Au(111) and polycrystalline Au foil over a wide range of temperatures (298–1123 K) and pressures (10^{-8}–10 Torr, 1.3×10^{-11}–0.013 atm) and found that no oxygen could be adsorbed at 298 K for all O_2 pressures. However, oxygen could be adsorbed on both surfaces at temperatures above 573 K for pressures not less than 1 Torr. Pireaux *et al.*[20] determined that O_2 does not dissociatively adsorb on gold surfaces under ultrahigh vacuum (UHV) conditions (10^{-10}–10^{-5} Torr, temperatures from 100 to 800 K), except when an impurity (Ca, Mg, and Si) is present. Canning *et al.*[18] studied the oxidation of gold in UHV and found that no oxygen adsorption was detected on a clean gold sample for oxygen pressures up to 10^{-4} Torr (1.316×10^{-7} atm) and sample temperatures in the range of 300–600 K. Chemisorption of oxygen atoms could be achieved, however, by placing a hot platinum filament close to the sample during exposure to oxygen. Pireaux *et al.*[21] formed gold oxide on Au(111) by oxygen dc reactive sputtering and demonstrated that the oxide is of the Au_2O_3 (auric oxide) form and that it decomposes under thermal treatment in the temperature range 390–590 K. It was assumed that Au_2O (aurous oxide) is a possible intermediate of this reduction.

A number of studies have employed ozone (O_3) to deposit atomic oxygen on Au(111) under UHV conditions[22–24] resulting in gold oxide formation. Such a film decomposed when heated to 423–473 K.[23] This is reasonably consistent with the reported decomposition temperature of 423 K for bulk Au_2O_3.[25] Saliba *et al.* also used ozone to deliver atomic oxygen to Au(111).[26] No ordered overlayer of oxygen on Au(111) was observed by low-energy electron diffraction, and an oxygen coverage as small as 0.1 ML (monolayer) was sufficient to lift the surface herringbone reconstruction of the clean (111) surface. Davis and Goodman[27] subsequently confirmed this result.

In contrast to most of the above-mentioned investigations, a number of studies have reported a "strongly bound" oxygen species on Au(111): Cao *et al.*[28] reported that a chemi-

sorbed state of oxygen on Au(111) was formed after O_2 exposure at a pressure of 5×10^{-6} mbar (3.75×10^{-6} Torr, 5×10^{-9} atm) and a temperature ranging from 873 to 1123 K. In addition, a twisted oxide (AuO_x) overlayer with a ($\sqrt{3} \times \sqrt{3})R30°$ periodicity was reported to form with further oxygen adsorption. Subsequent scanning tunneling microscopy studies[29–31] reproduced the ($\sqrt{3} \times \sqrt{3})R30°$ overlayer structure on Au(111), not under UHV conditions, but by applying an O_2 pressure of 1 bar (750 Torr, 0.98 atm) and temperatures between 500 and 800 °C (773–1073 K). These authors assigned this structure to "strongly chemisorbed oxygen." Uchida *et al.*[32] detected the formation of a long-range superstructure on the Au(111) surface following reaction with oxygen at atmospheric pressure and a temperature of about 1070 K using reflection electron microscopy. This superstructure exhibited unit cell dimensions of about 8.5 nm in the [112] direction and 4.9 nm in the [110] direction, and reflection high-energy diffraction patterns showed a ($\sqrt{3} \times \sqrt{3})R30°$ periodicity on the Au(111) surface. The nature of this surface structure remains unclear and bears a close resemblance to a similar $\sqrt{3}$ structure (also not yet understood) reported for O/Ag(111).[33,34]

More recently, there have been studies addressing the effect on the reactivity of preadsorbed atomic oxygen on Au(111) for certain chemical reactions; in particular, McClure *et al.*[35] employed molecular beam scattering techniques to investigate the adsorption and/or reaction of NO with an atomic oxygen covered Au(111) surface. Their results illustrate that while clean gold surfaces are generally catalytically inert, the presence of chemisorbed oxygen significantly increases the adsorption and/or reactive properties of Au(111) toward gas-phase nitric oxide. Temperature programed desorption was performed by Deng *et al.*[36] under a base pressure of 6×10^{-10} Torr (8×10^{-13} atm). They reported that the dissociation probability of O_2 on Au(111) is dramatically increased by the presence of some atomic oxygen on the surface. In particular, at 400 K, the dissociation probability of O_2 on an oxygen precovered Au(111) is of the order of 10^{-3}, whereas there is no measurable dissociation on clean Au(111). These authors proposed that the enhancement of O_2 dissociation is possibly due to the release of Au atoms from the surface (in particular, from the "elbows" in the herringbone structure) due to restructuring induced by atomic oxygen deposition;[36,37] this offers low-coordinated Au sites that may lower the dissociation barrier for O_2.

With regard to first-principles calculations for the O/Au(111) system, Mavrikakis *et al.*[11] carried out density-functional theory (DFT) calculations for the adsorption of O and CO on flat and stepped Au(111) surfaces. Steps were found to bind oxygen atoms considerably stronger than the terraces, and an expansive strain has a similar effect. They suggested that the unusually high catalytic activity of dispersed Au particles may in part be due to high step densities on the small particles and/or strain effects due to the mismatch at the Au-support interface. Liu *et al.*[38] performed calculations to investigate O atom adsorption and O_2 dissociation on Au(111), Au(211), and Au(221). They suggested that O_2 dissociation cannot occur at low temperatures due to large activation energy barriers. Xu and Mavrikakis[39] also

studied O_2 dissociation on strained and stepped gold surfaces and found that O_2 does not adsorb on Au(111) but does bind, albeit weakly, to a Au(111) surface stretched by 10%, as well as to Au(211) surfaces, both stretched and unstretched.

In this paper, we examine the interaction of atomic oxygen, and the stability of thin surface oxides, on Au(111) in the context that it may provide some insight into the catalytic behavior of gold. Similar studies have recently been performed for other transition metal systems, such as O/Ru(0001),[40,41] O/Rh(111),[42,43] O/Ir(111),[44] O/Pd(111),[45] O/Ag(111),[46–48] and O/Cu(111),[49] which generally show that surface oxide formation becomes more favorable at lower O coverages for the softer (more to the right of the Periodic Table) metals.[50] For O/Au(111), we find that this trend holds and surface oxide formation is always preferred over on-surface chemisorbed oxygen.

The paper is organized as follows. In Sec. II, we give details of the first-principles DFT total-energy calculations and definitions and describe the thermodynamical method. In Sec. III, results are presented for bulk Au, the clean Au(111) surface, and the O_2 molecule, while results for on-surface adsorption are presented in Sec. IV. Section V contains investigations of subsubsurface oxygen and "mixed" on-surface+subsurface structures, and in Sec. VI, results for thin surface-oxide-like configurations are presented, followed by the conclusion in Sec. VII. Convergence tests for the oxygen molecule and the adsorption energy are described in the Appendix, along with consideration of the vibrational contribution to the surface free energy of the most favorable surface-oxide-like structure.

II. CALCULATION METHOD AND DEFINITIONS

The calculations are performed using the DFT total-energy Vienna *ab initio* simulation package (VASP).[51–53] We employ the projector augmented-wave method[54,55] (PAW) and the generalized-gradient approximation (GGA) for the exchange-correlation functional.[56] The wave functions are expanded in a plane-wave basis set with an energy cutoff of 36.75 Ry (500 eV). The surface is modeled by a five-layer slab, separated by 15 Å of vacuum space. Oxygen is placed on one side of the slab where the induced dipole moment is taken into account by applying a dipole correction.[57] We allow atomic relaxation of all gold atoms in the top three layers of the slab plus the oxygen atoms. The final forces on the atoms are less than 0.01 eV/Å. For the **k**-point sampling, a $12 \times 12 \times 1$ mesh of (Γ-centered) points is used for the (1 $\times$ 1) surface unit cell (SUC), which generates 19 **k** points in the surface irreducible Brillouin zone (IBZ) for the Brillouin zone integration. Equivalent **k** points are used for all of the surface structures studied to maximize the accuracy. A Gaussian function is used with a temperature broadening of $k_B T^{el} = 0.2$ eV to improve the convergence (k_B is the Boltzmann constant) and the total energy is extrapolated to zero temperature. The PAW potential is generated taking scalar relativistic corrections into account.

The average adsorption energy per oxygen atom on the surface, $E_{ad}^{on-surf}$, is defined as

$$E_{ad}^{on\text{-}surf} = -\frac{1}{N_O}[E_{O/Au} - (E_{Au} + N_O E_O)], \quad (1)$$

where N_O is the number of oxygen atoms in the SUC, and $E_{O/Au}$, E_{Au}, and E_O represent the total energy of the adsorbate-substrate system, the clean surface, and the free oxygen atom, respectively. It is defined such that a positive number indicates that the adsorption is exothermic (stable) and a negative number indicates endothermic. The adsorption energy per oxygen atom can also be referenced to the energy which the O atom has in the O_2 molecule by subtracting half the binding energy $E_b^{O_2}$,

$$E_{ad[(1/2)O_2]}^{on\text{-}surf} = E_{ad}^{on\text{-}surf} - \frac{1}{2}E_b^{O_2}. \quad (2)$$

For the formation of a surface oxide, the average adsorption energy is

$$E_{ad}^{surf\text{-}oxide} = -\frac{1}{N_O}[E_{O/Au} - (E_{Au} + N_O E_O) + N_{Au}E_{Au}^{bulk}], \quad (3)$$

where N_{Au} is the number of Au atoms missing compared to the ideal five-layer Au(111) surface, and E_{Au}^{bulk} is the total energy of a gold atom in bulk. This term appears since the missing Au atoms are assumed to be rebound at kink sites at steps, which contribute an energy equal to that of a bulk Au atom.[58,59]

We consider the difference electron density

$$n^\Delta(\mathbf{r}) = n(\mathbf{r}) - n^0(\mathbf{r}) - n^O(\mathbf{r}), \quad (4)$$

where $n(\mathbf{r})$ is the total electron density of the adsorbate-substrate system, and $n^0(\mathbf{r})$ and $n^O(\mathbf{r})$ are the electron densities of the clean substrate and the free oxygen atom, respectively, where the atomic geometry of the substrate is that of the relaxed adsorbate system (but without the O atoms). This quantity then shows from which regions the electron density has been depleted and increased due to O adsorption on the surface.

We also consider the effect of temperature and pressure of the gas phase by "*ab initio* atomistic thermodynamics" (see, e.g., Refs. 60–65). Here, the combination of thermodynamics and DFT can be applied to obtain the lowest-energy surface structures with a surrounding gas phase, thus enabling the construction of a (T,p) phase diagram of the stability (or metastability) regions of different surface phases.

We consider the surface in contact with an oxygen atmosphere, which is described by an oxygen pressure p and a temperature T, and calculate the surface free energy as

$$\gamma(T,p) = (G_{O/Au(111)}^{slab} - G_{Au(111)}^{slab} + N_{Au}\mu_{Au} - N_O\mu_O)/A. \quad (5)$$

$G_{O/Au(111)}^{slab}$ and $G_{Au(111)}^{slab}$ are the Gibbs free energies of the O/Au surface under consideration and that of the clean Au(111) reference system, respectively. For oxygen on-surface and subsurface adsorption, the number of "missing gold atoms" (N_{Au}) is zero. μ_{Au} and μ_O are the chemical potentials of Au and O atoms, respectively, and A is the surface area. We take $\mu_{Au} = g_{Au\text{-}bulk}$, the free energy of a bulk Au atom. For pressures not exceeding about 100 atm, the contribution from the pV term in Gibbs free energy is negli-

gible. We investigated the magnitude of vibrational contributions for the lowest-energy structure (see Appendix) and found that they are unlikely to affect the conclusions drawn, similar to that reported for other systems (see, e.g., Ref. 66). Thus, the total energies are the dominant terms in the Gibbs free energies.

The T and p dependence is mainly given by μ_O, i.e., by the O_2 gas-phase atmosphere,

$$\mu_O(T,p) = \frac{1}{2}\left[E_{O_2}^{total} + \tilde{\mu}_{O_2}(T,p^0) + k_B T \ln\left(\frac{p_{O_2}}{p^0}\right)\right], \quad (6)$$

where p^0 corresponds to atmospheric pressure and $\tilde{\mu}_{O_2}(T,p^0)$ includes the contribution from rotations and vibrations of the molecule, as well as the ideal-gas entropy at 1 atm.[66] $E_{O_2}^{total}$ is the total energy of the oxygen molecule. For $\tilde{\mu}_{O_2}(T,p^0)$, we use the experimental values from thermodynamic tables.[67] The $T=0$ K value of Eq. (6) is

$$\mu_O(T=0\text{K},p) = \frac{1}{2}E_{O_2}^{total}. \quad (7)$$

We choose this to be the zero reference of $\mu_O(T,p)$ and call it the "oxygen-rich" condition. Then, we define $\Delta\mu_O = \mu_O - (1/2)E_{O_2}^{tot}$. The "oxygen-poor" value is then

$$\mu_O^{poor} = (1/2)E_{O_2}^{total} - H_{Au\text{-}oxide\ bulk}^f, \quad (8)$$

where $H_{Au\text{-}oxide\ bulk}^f$ is the heat of formation per O atom of the most stable gold oxide, which is Au_2O_3. If the oxygen chemical potential becomes lower (more negative) than μ_O^{poor}, the bulk oxide starts to decompose. We calculate $H_{Au\text{-}oxide\ bulk}^f = -(1/3)(E_{Au_2O_3}^{tot} - 2E_{Au}^{bulk} - 3/2E_{O_2}^{total})$ to be 0.173 eV per O atom (or 0.519 eV per stoichiometric unit).[68] Reported experimental values are also weakly exothermic: 0.135 eV,[69] 0.0937 eV,[70] and 0.0353 eV (Ref. 71) per stoichiometric unit at the standard state, i.e., room temperature and atmospheric pressure.

III. THE Au(111) SURFACE, BULK Au, AND THE OXYGEN MOLECULE

The calculated lattice constant of gold is 4.175 Å and the bulk modulus is 132 GPa. The corresponding experimental values are 4.08 Å and 170 GPa.[72] Thus, the DFT-GGA result slightly overestimates the former and, correspondingly, underestimates the latter. The calculated value agrees very well with previous DFT-GGA results, where values of 4.19 Å and 132 GPa were reported.[73] The theoretical (DFT-GGA) cohesive energy of Au is 3.05 eV/atom and the value reported from VASP using the local density approximation (LDA) is 4.39 eV/atom.[74] The experimental result is 3.81 eV/atom.[72] The GGA thus underestimates and the LDA overestimates the cohesive energy. In our GGA calculations, the free gold atom has been calculated including spin polarization.

For the ideal (unreconstructed) Au(111) surface, we first performed calculations using (1×1), (2×2), (3×3), and (4×4) surface unit cells. These calculations provide not only a test of the surface relaxations with cell size but are also used to evaluate the different electron densities. The varia-

tion of the work function is negligible between the different surface cells [5.274, 5.284, 5.284, and 5.279 eV for (4×4), (3×3), (2×2), and (1×1), respectively] and is similar to experiment (5.26 eV).[75] The first interlayer spacing is calculated to be expanded by 1.6%, and the second interlayer spacing contracts by 0.6%.

The binding energy of O_2, $E_b^{O_2}$, is 3.14 eV per O atom from DFT-GGA, the bond length $d_0 = 1.24$ Å, and the vibrational frequency $\omega = 193$ meV (1561 cm^{-1}). Convergence tests are described in the Appendix, which demonstrate that these values are highly converged. The experimental values are $(1/2)E_b^{O_2} = 2.56$ eV, $d_0 = 1.21$ Å, and $\omega = 196$ meV (1580 cm^{-1}).[76] The binding energy is therefore overestimated (which is well known). These values are typical of well-converged DFT-GGA calculations; similar values have been obtained by, e.g., Perdew *et al.*[77] $[(1/2)E_b^{O_2} = 3.12$ eV] and Li *et al.*[59] $[(1/2)E_b^{O_2} = 3.13$ eV].

IV. ON-SURFACE ADSORPTION

A. Energetics

For oxygen adsorption on the surface, we considered the hcp- and fcc-hollow sites, which are threefold-coordinated sites directly above second- and third-layer gold atoms, respectively, for a coverage range of 0.06 ML to a full monolayer. We used (4×4), (3×3), (2×2), and (1×1) SUCs for coverages of 0.06, 0.11, 0.25, and 1.0 ML, respectively. Coverages of 0.5 and 0.75 ML were calculated in the (2×2) SUC containing two and three oxygen atoms, respectively. Equivalent **k** points are used for all systems, which leads to 3, 4, 7, 13, 7, and 19 points in the surface IBZ for coverages of 0.06, 0.11, 0.25, 0.50, 0.75, and 1.0 ML. For the 0.50 ML structure, which has a (2×1) arrangement of O atoms in the (2×2) surface cell, the number of **k** points increases due to the lower symmetry. The energetically most favorable adsorption site is the fcc-hollow site, as is the case on the (111) faces of other fcc transition metals.[59,78–80] The hcp-hollow site is systematically higher in energy than the fcc site by an average of 0.181 eV. The adsorption energies for O in the fcc site, with respect to atomic oxygen, are plotted in Fig. 1 and the values are given in Table I.

The adsorption energy significantly decreases for coverages greater than 0.25 ML, which indicates that a strong repulsive interaction between adsorbates builds up. Considering the adsorption energy with respect to half the binding energy of the theoretical O_2 molecule, the calculations predict that only for coverages of 0.25 ML and less is O adsorption stable. With respect to the experimental value, coverages less than ≈0.7 ML are stable. We note that an energy barrier to associative desorption may exist, which could keep the O atoms on the surface, even though the energy of O_2 in the gas phase may be lower.

The interaction between O and Au(111) is weaker than that between O and other transition metals: For a coverage of 0.25 ML, the adsorption energies are 5.55, 5.22, 4.97, 4.69, 4.57, and 3.52 eV for O/Ru(0001),[81,82] O/Rh(111),[43] O/Ir(111),[44] O/Cu(111),[49] O/Pd(111),[45] and O/Ag(111),[59] respectively, as compared to the value of 3.25 eV for O/Au(111).
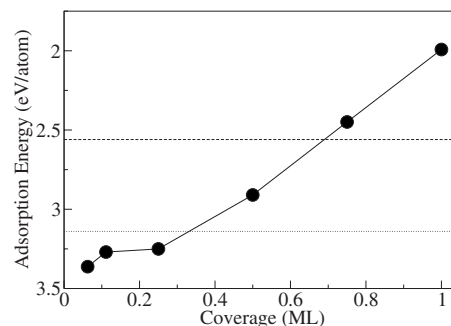
FIG. 1. Calculated adsorption energy of oxygen on Au(111) in the fcc-hollow site versus coverages with respect to atomic oxygen. The upper and lower horizontal lines represent the experimental (2.56 eV) and theoretical (3.14 eV) values of the O_2 binding energy per atom. The solid line is to guide the eyes.

B. Atomic structure

The O-Au bond lengths, and vertical interlayer distances, of oxygen in the fcc site on Au(111) for the different coverages are listed in Table I. The O–metal bond length does not change appreciably as a function of coverage for 0.06–0.75 ML. It varies only from 2.12 Å (for 0.25 ML) to 2.18 Å (for 0.75 ML). With regard to the vertical O-Au(111) interlayer distance, however, it can be seen that for 1 ML, it becomes notably larger with a value of 1.35 Å, and at coverage 0.5 ML, it is smaller (1.03 Å) than the distances for 0.25 and 0.50 ML (of 1.17 Å). The first interlayer spacing for O/Au(111) for the different coverages is also very similar to that of the clean surface, i.e., expanded by 1.7%, with the exception of the 1.0 ML structure, where it is *contracted* by 3.7%. With regard to lateral relaxations, for the 0.06, 0.11, and 0.25 ML structures, the three Au atoms bonded to the O atom move radially outward from chemisorbed oxygen by, on average, 0.14 Å. For a coverage of 0.50 ML, the distortion is anisotropic due to the lower symmetry. The gold atoms which bond to two oxygen atoms are displaced away from the bulk-terminated positions by 0.24 Å along the [120] direction, while the gold atoms that are bonded to just one O atom move 0.17 Å in the opposite direction, i.e., along [$\bar{1}$20]. The oxygen atom also displaces along the [$\bar{1}$20] direction, away from its ideal fcc-hollow site center by 0.19 Å. For 0.75 ML coverage, one surface gold atom is bonded to three oxygen atoms, and due to symmetry, its position is laterally fixed. The three remaining gold atoms in the surface unit cell are bonded to two oxygen atoms and displaced radially inward toward each other, i.e., toward the vacant fcc site, by 0.17 Å. The three O atoms are displaced by 0.06 Å radially outward, away from the first-mentioned fixed Au atom. These displacements are very similar to those for O/Ag(111).[59]

C. Electronic properties

1. Work-function change and surface dipole moment

We now turn to analyze the electronic properties of the O/Au(111) system, first considering the change in the work

TABLE I. Calculated structural parameters (in Å) for various coverages for O in the fcc-hollow site. R_1 indicates the bond length between oxygen and the nearest-neighbor gold atom, $d_{O\text{-}Au}$ is the vertical height of oxygen above the topmost gold layer, and d_{12} and d_{23} are the first and second metal interlayer distances, where the center of mass of the layer is used. The calculated interlayer distance for bulk is 2.41 Å. $E_{ad}^{on\text{-}surf}$ is the adsorption energy in eV with respect to atomic oxygen. For the 0.50 and 0.75 ML structures, there are two different O-Au bond lengths; in the table, we present the average of these.

Coverage	R_1	$d_{O\text{-}Au}$	d_{12}	d_{23}	$E_{ad}^{on\text{-}surf}$
0.06	2.15	1.04	2.44	2.39	3.36
0.11	2.15	1.12	2.43	2.39	3.27
0.25	2.12	1.17	2.44	2.40	3.25
0.50	2.13	1.03	2.64	2.40	2.91
0.75	2.18	1.17	2.44	2.39	2.45
1.00	2.17	1.35	2.32	2.39	1.99

function with O coverage. The results are shown in Fig. 2 (upper). It can be seen that the work function increases with coverage, and saturation is not reached. The increase is due to a large (inward pointing) surface dipole moment arising from a significant electron transfer from the substrate to the adatom. The large work-function increase can be expected on the basis of the large difference in electronegativity between oxygen (3.44) and gold (2.54). This behavior is similar to O/Ag(111) (Ref. 59) and O/Cu(111),[49] where at 1 ML coverage, the work function increases by almost 4.0 eV for both these systems compared to 2.6 eV for O/Au(111). The larger work-function change for O/Ag(111) and O/Cu(111) corresponds to the greater difference between the electronegativities of oxygen (3.44) and silver (1.93) and oxygen and copper (1.90). It is interesting to see from Fig. 2 (lower) that

FIG. 2. Change in the calculated work function $\Delta\Phi$ (upper) and surface dipole moment μ (lower) as a function of coverage for O in the fcc-hollow site on Au(111).

the surface dipole moment does not continue to decrease with increasing coverage beyond 0.5 ML; such a decrease, as is observed for other O/transition-metal systems [e.g., O/Ru(0001),[40,41] O/Rh(111),[42,43] O/Pd(111),[45] O/Ag(111),[48] and O/Cu(111) (Ref. 49)] may be expected due to depolarization of the O atoms in order to reduce the repulsive electrostatic interactions that build up between the partially negatively charged ions. With the understanding that the surface dipole moment can be viewed as being proportional to the product of the effective charge on the O atom and the vertical distance between O and Au(111), we have evaluated this quantity using the relative effective charge as obtained from the atom projected density of states (of 4.797, 4.859, and 4.848 for the 1.0, 0.50, and 0.25 ML structures). Using the vertical O-Au(111) displacements of 1.35, 1.03, and 1.17 Å for the 1.0, 0.50, and 0.25 ML overlayers, we obtain 6.476, 5.005, and 5.67, respectively. This trend is the same as exhibited by the surface dipole moment and is mainly due to the vertical O-Au(111) distances, even though there is a slight depolarization of the electron density of the O atoms of the 1.0 ML structure. We find, however, that this simple model cannot explain the behavior of the dipole moment in the low coverage regime of 0.06–0.25 ML where it initially increases then decreases as the relative effective O charge is rather similar but the vertical O-Au(111) distances increase. For all the other O/transition-metal (TM) systems noted above, the vertical O-substrate distance does not display a notable increase for the 1 ML structure. The O/Ag(111) and O/Cu(111) systems are the only ones that do exhibit a modestly larger O-substrate distance for the full monolayer structure (of 0.08 and 0.09 Å relative to the 0.50 ML case), but this is not large enough to result in an increase in the surface dipole moment for the full monolayer structure. Interestingly, it can also be seen from Table I that the first Au-Au interlayer spacing is notably contracted for the 1.0 ML structure with respect to the bulk interlayer distance (by ~4%), whereas it is expanded for the lower coverages. O/Ag(111) and O/Pd(111) are the only other systems mentioned above which also exhibit a contraction for the 1.0 ML structure, but for these it is only contracted by 1%–2%.
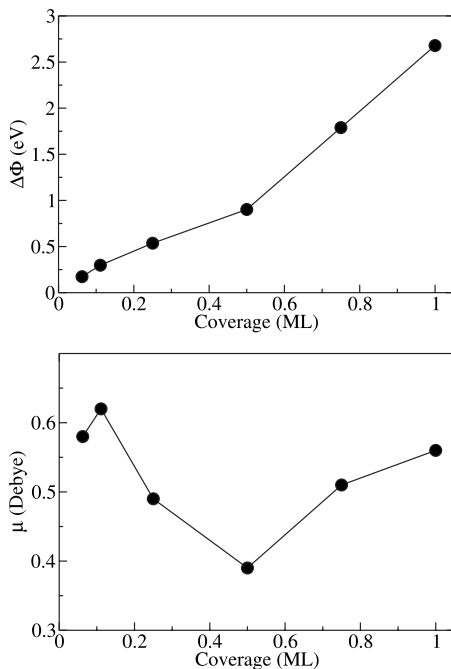
2. Difference electron density

To gain more insight into the nature of the bonding, we consider the difference electron density and projected density

FIG. 3. Difference electron densities for O in the fcc-hollow site on Au(111) for coverages of 0.06, 0.11, 0.25, and 1.0 ML. The dark isosurfaces indicate an increase in electron density, and the light isosurfaces represent a depletion. The black spheres represent the position of the oxygen and gold atoms. The value of the isospheres is $\pm 7.5 \times 10^{-5}$ $e/\text{Å}^3$.

of states (PDOS). The difference densities are shown in Fig. 3. Several points can be noted: First, the perturbation of oxygen adsorption to the substrate is mainly in the topmost gold layer, where the electron density around the gold atoms is depleted, in particular, from the Au $4d_{xz,yz}$-like orbitals. Second, there is a significant enhancement of electron density at the O atoms and also a polarization. It is obvious that the shape and magnitude of the difference electron density distributions are very similar for coverages of 0.06, 0.11, and 0.25 ML, indicating a similar bonding nature. That for coverage of 1.0 ML appears somewhat different because the O atoms bond to Au atoms that are also bonded to other O atoms. This gives rise to an Au-mediated lateral O-O interaction, as indicated by the increased electron density in the O $2p_{x,y}$-like states.

The PDOS are given in Fig. 4. It can be seen that there is a hybridization between O $2p$ and Au $5d$ orbitals for all the coverages considered. The PDOS for the O atom shows that there are two main regions of high electron density below the Fermi level. These correspond to bonding- and antibonding-like states. The bonding states are located near the bottom of the Au $5d$ band, and the antibonding states near the top of it are largely occupied, thus preventing a strong covalent bonding. For coverage of 1 ML, there is an antibonding state with a very high density of states (DOS) at the Fermi energy which further destabilizes the system, in accordance with the decrease in adsorption energy.

V. SUBSURFACE OXYGEN AND ON-SURFACE +SUBSURFACE STRUCTURES

In the subsurface region, there are three high-symmetry sites: the octahedral site and two tetrahedral sites. These are
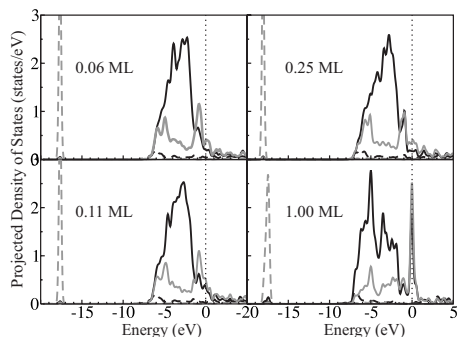
FIG. 4. Projected density of states for oxygen adsorbed on the surface for various coverages. The dark continuous and dashed lines indicate the Au $5d$ and $6s$ states, respectively, and the gray continuous and dashed lines represent the O $2p$ and $2s$ states, respectively.
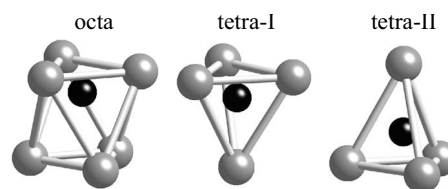
FIG. 5. Sites considered for subsurface adsorption of O under the first Au(111) layer. Dark and light spheres represent oxygen and gold atoms, respectively. The atoms are depicted in the relaxed positions.

denoted as "octa," "tetra-I," and "tetra-II" as depicted in Fig. 5. We performed calculations for oxygen in these different sites for 0.25 ML coverage. We also calculated several mixed on-surface+subsurface geometries that have been identified as low-energy configurations for other O/transition-metal systems.[50] All these calculations were performed using a (2 ×2) surface unit cell. Specifically, the mixed configurations consist of (a) one oxygen atom on the surface in the fcc site and one under the surface in the tetra-I site for 0.5 ML ($O_{\text{fcc}}/O_{\text{tetra-I}}$), (b) the same as (a) except there is an additional oxygen atom under the first Au layer in the tetra-II site for coverage of 0.75 ML ($O_{\text{fcc}}/O_{\text{tetra-I}}+O_{\text{tetra-II}}$), and (c) the same as (b) except two additional oxygen atoms are under the second Au layer in the tetra-I and tetra-II sites ($O_{\text{fcc}}/O_{\text{tetra-I}}+O_{\text{tetra-II}}/O_{\text{tetra-I}}+O_{\text{tetra-II}}$) for coverage of 1.25 ML. These structures are depicted in Fig. 6. We also tested in excess of 16 surface-oxide-like configurations in a (2×2) cell involving coverages from 0.25 to 0.75 ML, but all were notably less favorable than the (2×2) structures described above—with the exception of one structure: This configuration involves O in the fcc site plus a surface Au vacancy. This structure is depicted in Fig. 7. Here, it is assumed that the ejected surface Au atoms rebind at kink sites at steps where they gain the cohesive energy. That this structure is more favorable than O adsorption in the fcc site on the unreconstructed surface also gives further support to the experimentally reported "O-induced release of Au atoms."

A. Energetics

For the pure subsurface structures, the tetra-I site is most favorable; it is 0.22 and 0.66 eV more stable than the octa and tetra-II sites, respectively. Compared to adsorption on the surface in the fcc site, pure subsurface adsorption is significantly less favorable at the same coverage of 0.25 ML—by more than 0.8 eV. From Table II, it can be seen that the most favorable structure, as calculated in the (2×2) surface unit cell, is the one with O on the surface in the fcc site plus a vacant surface Au atom. This indicates that O adsorption on Au(111) can induce the ejection of Au atoms which may diffuse and adsorb at kink sites at steps, or bind to other adparticles on the surface.

The mixed on-surface+subsurface structures at higher coverage are more favorable than pure on-surface adsorption in the fcc site at the same coverage. Specifically, for 0.5 ML, the $O_{\text{fcc}}/O_{\text{tetra-I}}$ is more favorable per O atom by 0.31 eV, and for 0.75 ML, the $O_{\text{fcc}}/O_{\text{tetra-I}}+O_{\text{tetra-II}}$ structure is more

(a) 3.22 eV/0.50 ML

24.0 %

0.8 %

(b) 3.09 eV/0.75 ML

49.1 %

0.2 %

(c) 3.01 eV/1.25 ML

51.1 %

46.6 %
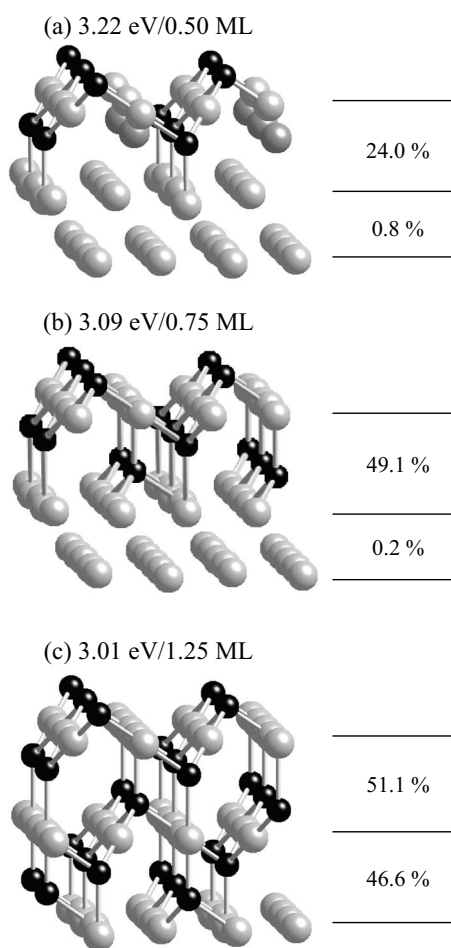
FIG. 6. Atomic geometry of on-surface+subsurface structures: (a) oxygen in the fcc site plus subsurface oxygen in the tetra-I site, (b) as for (a) but with additional oxygen in the tetra-II site, and (c) as for (b) but with additional oxygen under the second Au layer in the tetra-I and tetra-II sites. The average adsorption energy, with respect to free oxygen atoms, as well as the corresponding coverage are given. The relative variation of the first and second interlayer spacings, with respect to the value of the corresponding relaxed Au(111) surface, is also given. Large pale gray and small dark circles represent gold and oxygen atoms, respectively.

FIG. 7. Atomic geometry of a structure with O in the fcc-hollow site and a surface Au vacancy in a (2×2) cell. The surface unit cells are indicated. The oxygen atoms are represented by small dark circles, the uppermost Au atoms by small gray circles, and the intact plane of Au(111) atoms lying below by larger pale gray circles.

to coverages of slightly less than 0.5 ML is more stable. However, considering surface oxide structures using larger (4×4) surface unit cells, it is found that they are more favorable than oxygen chemisorption on the surface for *any* of the coverages considered (0.06–1 ML).[49] Similar results have subsequently been found for (4×4)-O/Ag(111) structures,[47] and as shown in Sec. VI below, it is also the case for O/Au(111).

To gain insight into the possibility of surface oxide formation via penetration of oxygen into the Au(111) surface, we calculated the energy barrier to pass through the first surface layer. We did this using a (2×2) surface unit cell and placed one oxygen atom in the (111) plane, coordinated to three Au atoms, and fixed the vertical positions of oxygen and the three neighboring Au atoms to be at the same height (if this was not done, on atomic relaxation, the O atom would "slip" back to the surface). We relaxed the positions of all other atoms. The resulting energy barrier for O going from an on-surface hollow site, through the first Au(111) layer,

favorable by 0.64 eV per O atom. The average adsorption energies are listed in Table II.

Interestingly, the adsorption energy of on-surface oxygen in the fcc site at 0.25 ML is only 0.03 eV more stable than that of the $O_{fcc}/O_{tetra-I}$ structure at 0.5 ML. This indicates that for O at the Au(111) surface, for coverages greater than 0.25 ML, oxygen would rather be in a such a "surface-oxide-like" structure than chemisorbed on the surface. A recent study of the incorporation of O into the basal plane of the late 4d TMs from Ru to Ag (Ref. 50) found that penetration starts after a critical coverage on the surface. This coverage was found to be lower for the softer metals toward the right of the TM series (Ag), in which the critical coverage is around 0.25 ML. It appears therefore that gold behaves similarly to Ag in this respect. We note that for oxygen on Cu(111), when considering surface oxides in (2×2) cells, as discussed above for the 4d TMs, adsorption on the surface up

TABLE II. Average adsorption energies per O atom, E_{ad}, for on-surface adsorption in fcc sites and pure subsurface adsorption in the three interstitial sites shown in Fig. 5. Also shown are the values for the on-surface+subsurface structures, as well as the (2×2) structure with O adsorbed in the fcc site and a surface Au vacancy. Values are given with respect to the free oxygen atom.

Adsorption energy (coverage)	(eV)
O_{octa} (0.25 ML)	2.18
$O_{tetra-I}$ (0.25 ML)	2.40
$O_{tetra-II}$ (0.25 ML)	1.75
$O_{fcc}/O_{tetra-I}$ (0.5 ML)	3.22
$O_{fcc}/O_{tetra-I}+O_{tetra-II}$ (0.75 ML)	3.09
$O_{fcc}/O_{tetra-I}/O_{tetra-II}/O_{tetra-I}+O_{tetra-II}$ (1.25 ML)	3.01
O on surface (0.25 ML)	3.25
O on surface (0.5 ML)	2.91
O on surface (0.75 ML)	2.45
O on-surface+Au-vacancy (0.25 ML)	3.31

and adsorbing in the subsurface tetra-I site is rather large, namely, 1.41 eV, particularly for low temperatures. This suggests that the identified surface-oxide-like structures do not form by O penetrating the ideal Au(111) surface, but possibly by Au atom diffusion from step edges or ejected Au atoms from the surface to combine with adsorbed O atoms. We calculated the diffusion barrier for O on Au(111) to be 0.17 eV using the difference in adsorption energy of O in the fcc and bridge sites. This small value indicates that O atoms are very mobile on the surface. Earlier *ab intito* calculations report the diffusion barrier of Au on Au(111) to be 0.22 eV,[83] so the Au atoms are also very mobile. To approximate the activation energy barrier for Au atoms to diffuse from step edges (where they have the cohesive energy of bulk Au) to the flat terrace, in order to combine with adsorbed on-surface O atoms, we consider the energy of Au on the bridge site on Au(111) plus the (2×2)-O structure. It is calculated to be 0.80 eV (relative to Au in bulk). If instead we consider that the Au atoms are ejected from the (2×2)-O structure [to result in the (2×2)-O+Au-vac structure plus a Au atom at the bridge site on Au(111)], the barrier is a little less, namely, 0.74 eV. With values such as this, it is possible that at around 300–400 K, restructuring could readily occur. We expect that the energy barriers for the experimentally observed ejection of Au atoms from elbows of the herringbone structure may be even less.

B. Atomic structure

Pure subsurface adsorption in the tetra-I site for coverage of 0.25 ML induces an (average) expansion of the first Au-Au interlayer spacing of 0.35 Å or (14.4%) relative to that of the relaxed Au(111) surface, similar to what has been found for other O/TM systems. The O-Au bond length between O and the first-layer Au atoms is 2.06 Å, and between O and the second Au layer, it is 2.32 Å. These values can be compared to the bond length of O on the surface in the fcc site, which is 2.12 Å. This suggests a stronger coupling of subsurface O to the first-layer Au atoms, which are effectively less coordinated due to the considerable expansion of the interlayer spacing. The $O_{fcc}/O_{tetra-I}$ system, for coverage of 0.5 ML, induces a larger (average) expansion of the first Au-Au interlayer spacing of 0.59 Å or (24.0%) relative to that of the relaxed Au(111) surface [see Fig. 6(a)]. The O-Au bond length between subsurface O and the first-layer Au atoms is 2.06 Å, and that between subsurface O and the second-layer Au atom is 2.32 Å—very similar to that described above for no oxygen on the surface. The bond length between the O on the surface and the first Au layer is 2.05 Å—notably shorter than for O only in the on-surface fcc site (2.12 Å), indicating a stronger bonding.

The $O_{fcc}/O_{tetra-I}+O_{tetra-II}$ and $O_{fcc}/O_{tetra-I}+O_{tetra-II}/O_{tetra-I}+O_{tetra-II}$ systems [see Figs. 6(b) and 6(c)] for coverages of 0.75 and 1.25 ML induce significant (average) expansions of the first Au-Au interlay spacing of 49.1% and 51.1% relative to that of the relaxed Au(111) surface, respectively. For the $O_{fcc}/O_{tetra-I}+O_{tetra-II}$ structure, the addition of the $O_{tetra-II}$ atom to the $O_{fcc}/O_{tetra-I}$ structure site does not result in any significant change in the O-Au bond lengths involving the
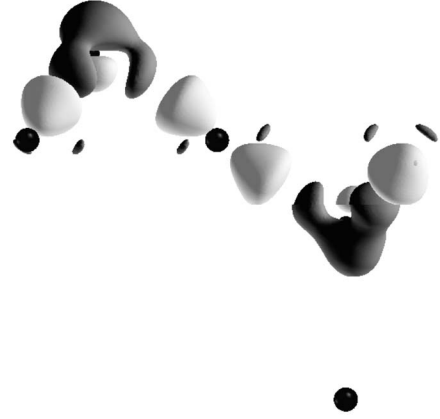
FIG. 8. The difference electron density $n^{\Delta}(\mathbf{r})$ [see Eq. (4)] for the on-surface+subsurface structure, $(O_{fcc}/O_{tetra-I})_{\theta=0.5}$. Dark and light regions represent electron enhancement and depletion, respectively. The values of the isospheres are $\pm 7.5 \times 10^{-5}$ $e/\text{Å}^3$. The positions of the O and Au atoms are indicated by black dots.

uppermost Au atom. However, consistent with the increased expansion of the first interlayer spacing, the bond length of subsurface $O_{tetra-I}$ to the second-layer Au atom is elongated to 2.58 Å. For $O_{tetra-II}$, the distance to the Au atom in the first layer is 2.35 Å, while the three equivalent bonds of $O_{tetra-II}$ to the Au atoms in the second layer are shorter (2.17 Å). Given these distances, it indicates that the *single* O-Au bonds [between Au(first layer)-$O_{tetra-II}$ and the $O_{tetra-I}$-Au (second layer)] are notably weaker compared to the alternative three equivalent bonds of oxygen to the gold atoms of each respective layer (see Fig. 6). In other words, the "intraplanar" bonding within an O-Au-O "trilayer" is stronger than the interlayer bonds between the trilayers. The bond lengths for the $O_{fcc}/O_{tetra-I}+O_{tetra-II}/O_{tetra-I}+O_{tetra-II}$ structure are very similar to those for the $O_{fcc}/O_{tetra-I}+O_{tetra-II}$ structure.

C. Electronic properties

In Fig. 8, we show the difference electron density distribution for the $O_{fcc}/O_{tetra-I}$ structure. A depletion of Au $5d_{xz,yz}$ states of the surface gold atoms bonded to the on-surface and subsurface oxygen atoms is evident, while there is an increase in electron density, and a polarization, on the O atoms. The coupling between subsurface O and the gold atom directly below in the second metal layer is weak, as indicated by the weak (absent) perturbation of electron density, consistent with the longer bond length described above.

In Fig. 9, the projected density of states is shown for subsurface oxygen in the tetra-I site and of the first- and second-layer gold atoms which are bonded to it. Compared to the PDOS for O on the surface (0.25 ML, Fig. 4), we find that the Au $5d$ band of the first Au layer is narrower, consistent with its reduced coordination. The O-Au bonding states are about 0.7 eV lower in energy compared to adsorption on the surface and they now appear outside the main Au $5d$ band. Furthermore, the O-related DOS over the whole energy range is smaller relative to the Au-derived ones for the sub-
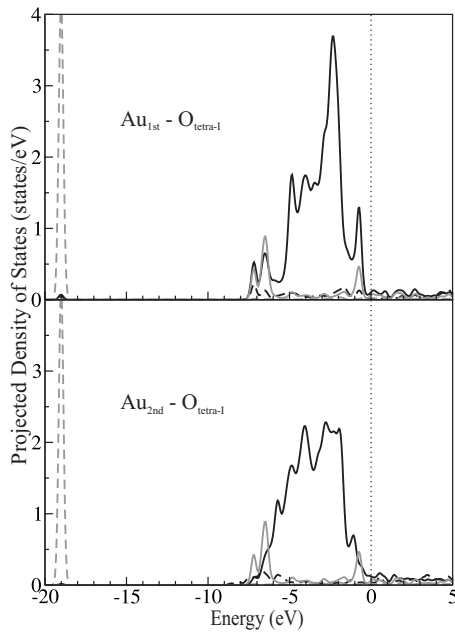
FIG. 9. Projected density of states for the pure subsurface tetra-I structure. The dark lines indicate the Au PDOS of the first metal layer atoms that are bonded to oxygen (top) and the Au PDOS of the second metal layer atoms that are beneath oxygen (bottom). The Au 6s orbital is indicated by the dashed dark line, the Au 5d orbital by the solid dark line, the O 2s orbital by the dashed gray line, and the O 2p orbital by the solid gray line. The Fermi energy is indicated by the vertical line.
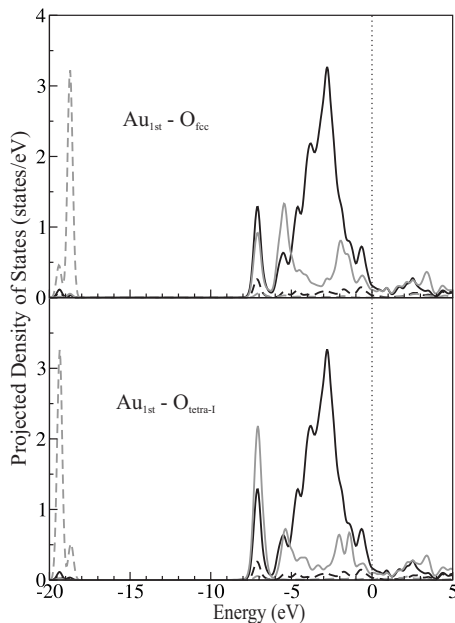
FIG. 10. Projected density of states for the O_{fcc}-Au-$O_{tetra-I}$ structure. The Au PDOS of the first metal layer atoms that are bonded to oxygen is indicated by dashed (6s) and solid (5d) dark lines, respectively. The gray lines denote the PDOS of O in the fcc site (upper) and tetra-I site (lower). The O 2s and 2p orbitals are indicated by the dashed and solid gray lines, respectively. The Fermi energy is represented by the vertical line.
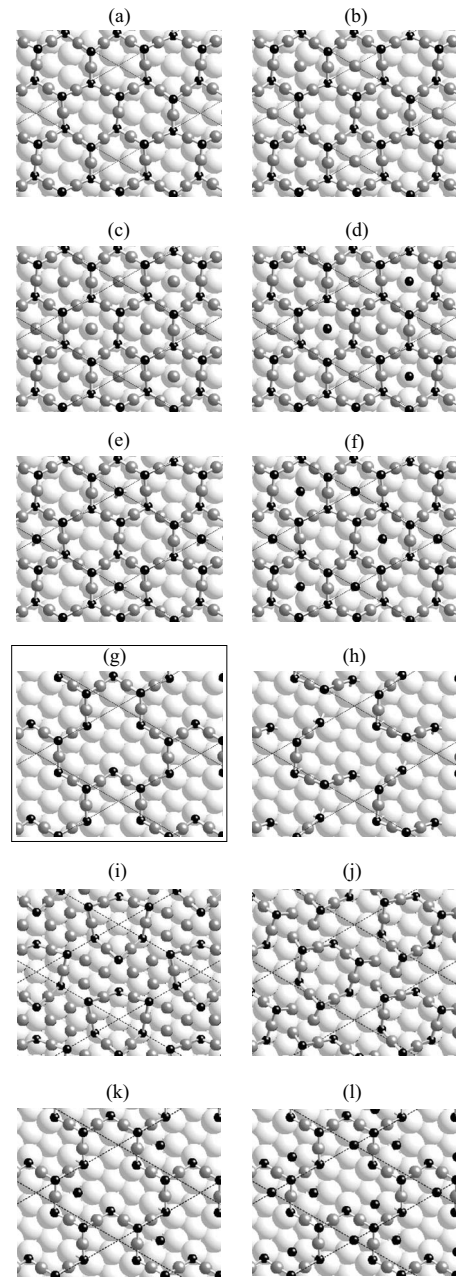
FIG. 11. Atomic geometry of surface-oxide-like structures on Au(111) calculated using (4×4) surface unit cells (indicated). The oxygen atoms are represented by small dark circles, the uppermost Au atoms by gray circles, and the intact plane of Au(111) atoms lying below by the larger paler gray circles. The lowest-energy structure (g) is framed.

surface structure, and the antibonding states are more occupied as compared to on-surface oxygen. This results in the weaker interaction of oxygen with the substrate. This behavior is similar to what has been observed for the O/Ag system.[48]

Figure 10 shows the PDOS for the $O_{fcc}/O_{tetra-I}$ structure. With the O_{fcc}-Au-$O_{tetra-I}$ linear coordination, the coupling between both O atoms and the surface Au atom becomes stronger as indicated by the greater electron density of the bonding state between O 2p and Au 5d orbitals and greater

TABLE III. Average adsorption energy $E_{ad}^{surf\text{-}oxide}$ per O atom for the surface-oxide-like structures shown in Fig. 11. All energies are given with respect to the free oxygen atom. Also given is the number of O atoms (N_O) and number of topmost Au atoms ($N_{Au\text{-}surf}$) in the (4×4) surface unit cell, the corresponding coverage, and the ratio of O atoms to Au atoms ($N_{Au\text{-}surf}$) in the surface-oxide-like layer.

Structure	$N_O:N_{Au\text{-}surf}$	N_O	$N_{Au\text{-}surf}$	Coverage (ML)	$E_{ad}^{surf\text{-}oxide}$ (eV)
(a)	0.666	6	9	0.375	3.46
(b)	0.545	6	11	0.375	3.33
(c)	0.500	6	12	0.375	3.18
(d)	0.636	7	11	0.4375	3.16
(e)	0.778	7	9	0.4375	3.42
(f)	0.889	8	9	0.50	3.34
(g)	0.833	5	6	0.3125	3.54
(h)	1.250	5	4	0.3125	3.26
(i)	0.500	6	12	0.375	3.08
(j)	0.667	6	9	0.375	3.31
(k)	1.000	6	6	0.375	3.39
(l)	1.333	8	6	0.50	3.29

overlap (hybridization) of these states throughout the whole energy range. Consequently, the binding of oxygen in this structure is stronger compared to pure subsurface or even pure on-surface oxygen at the same coverage.

VI. THIN SURFACE-OXIDE-LIKE STRUCTURES

In this section, we consider additional surface-oxide-like structures that are not constrained as much as the structures discussed above studied using (2×2) SUCs. In particular, we investigate 12 configurations using (4×4) SUCs. These configurations were stimulated by earlier studies for the O/Ag(111) and O/Cu(111) systems[47–49] and are depicted in Fig. 11. Specifically, we investigated (a) a honeycomb structure with six O and nine Au atoms in the surface layer; (b) as for (a) but with additional Au atoms in the fcc and hcp sites; (c) as for (b) but with an additional Au in the top site; (d) as for (b) but with an additional O atom in the top site; (e) as for (a) the honeycomb configuration but with an additional O atom in the fcc site; (f) as for (e) but with one more O atom in the hcp site; (g) as for (a) the honeycomb structure but removing three Au atoms and one O atom from the unit cell; and (h) as for (g) but removing two further Au atoms which are located in quasi-top-sites. The structure in Fig. 11(i) is analogous to that recently reported for the (4×4)-O/Ag(111) phase,[84,85] and (j) is as for (i) but with three less Au atoms in the surface unit cell. The structures shown in (k) and (l) are as for (g), but with one and three additional O atoms in the fcc sites, respectively. The average adsorption energies (per O atm) of these configurations are presented in Table III. It can be seen that structure (g) has the most favorable energy, with structure (a), the honeycomb configuration, the next most favorable.

The calculated difference electron density distribution for the lowest-energy surface oxide structure [Fig. 11(g)] is shown in Fig. 12. Qualitatively, the features are very similar

to the O_{fcc}-Au-$O_{tetra\text{-}I}$ structure described above (shown in Fig. 10), with a depletion of the Au 5d states and an increase in the O 2p states, as well as a polarization of the O atoms. In Fig. 13, we show the corresponding PDOS. Again, qualitatively, they are similar to those of the O_{fcc}-Au-$O_{tetra\text{-}I}$ structure described above. It is interesting to note that the work-function change of the lowest-energy (4×4) surface-oxide-like structure in Fig. 11(g) is *negative*, i.e., −0.31 eV, in contrast to the large positive changes induced by on-surface oxygen.
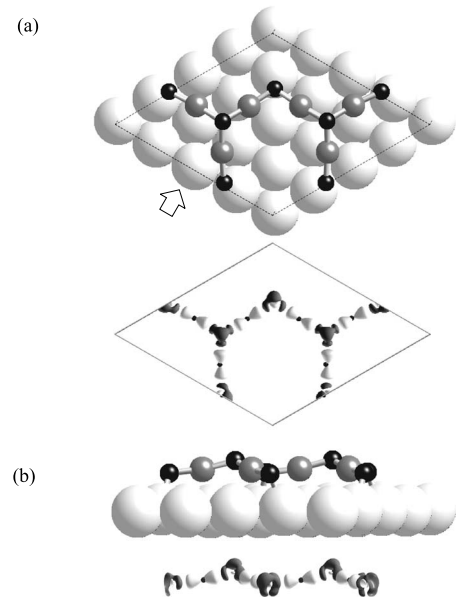
FIG. 12. Difference electron density $n^\Delta(\mathbf{r})$ [see Eq. (4)] for the lowest-energy surface-oxide-like structure [Fig. 11(g)]. The (4×4) surface unit cell is indicated by the line. (a) Top view and (b) side view.
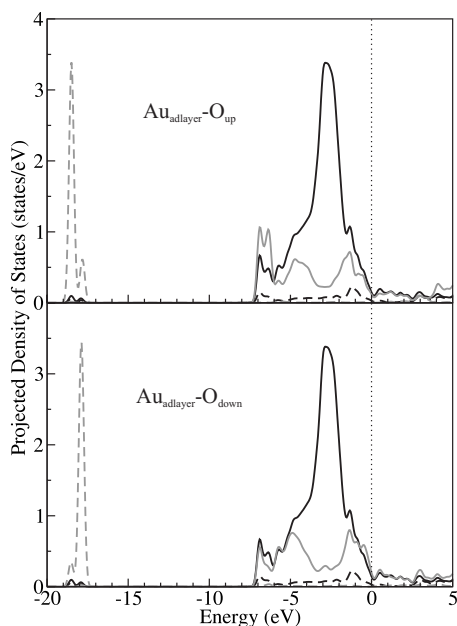
FIG. 13. Projected density of states for the lowest-energy surface-oxide-like structure [Fig. 11(g)]. The Au PDOS of the first metal layer atoms that are bonded to oxygen is indicated by dashed ($6s$) and solid ($5d$) dark lines, respectively. The gray lines denote the PDOS of O at upper and lower sites. The O $2s$ and $2p$ orbitals are represented by the dashed and solid gray lines, respectively. The Fermi energy is represented by the vertical line.

In Fig. 14, we show the surface free energies for the most favorable structures considered, along with on-surface chemisorption for comparison. The steeper the gradient, the higher the O coverage. Using Eq. (6), we correlate the oxygen chemical potential with temperatures for two selected
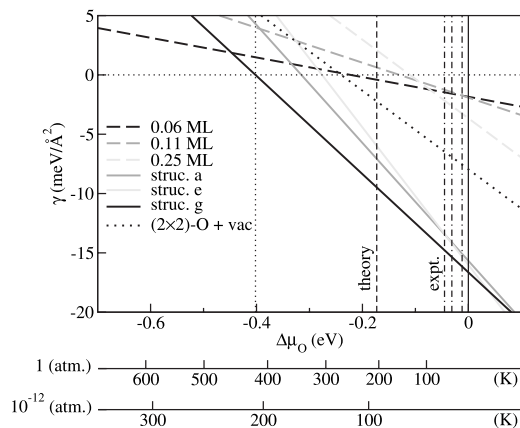
FIG. 14. Surface free energies for O at Au(111) for the various low-energy structures as a function of the O chemical potential, where $\Delta\mu_O$ is defined as $\mu_O - (1/2)E_{O_2}^{total}$. On-surface chemisorbed oxygen with coverages of 0.06, 0.11, and 0.25 ML, the (4×4) surface-oxide structures shown in Figs. 11(a), 11(e), and 11(g), (labeled "struc. a," etc.), and the (2×2)-O+vac structure (cf. Fig. 7) are presented. The corresponding temperatures are given for two selected pressures [see Eq. (6)], one corresponding to UHV conditions and the other to atmospheric pressure.
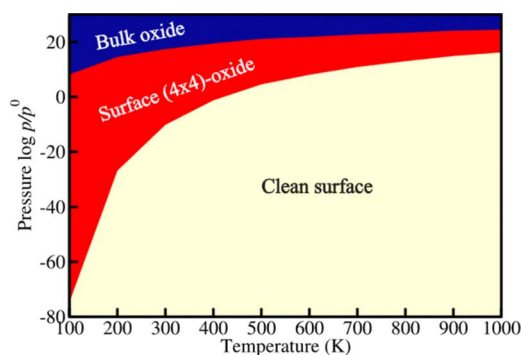
FIG. 15. (Color online) The calculated pressure-temperature phase diagram for O/Au(111) where the ranges of stability of the various phases are indicated.

pressures, namely, that which corresponds to UHV and the other characteristic of atmospheric pressure employed in catalysis. It can be seen that on-surface O is only metastable, and the thin surface-oxide-like structure shown in Fig. 11(g) is predicted to be stable for values of μ_O from -0.17 to -0.4 eV, which correspond to a temperature region of 200–420 K at a pressure of 1 atm; for a low pressure of 10^{-12} atm $(7.6\times10^{-9}$ Torr), this structure would only be stable for $T \leqslant 200$ K. Using Eq. (6), the above results can be presented as the two-dimensional phase diagram as shown in Fig. 15, where the stability regime of the (4×4) thin surface-oxide-like structure can be seen. The finding that such a structure is predicted to be stable under conditions at which low-temperature gold-based catalysts are active raises the question of whether such thin surface-oxide-like configurations could play a role in the high catalytic activity of gold nanoparticles. In a forthcoming paper, we investigate the reactivity of this surface for CO oxidation.

VII. CONCLUSIONS

We have studied the O/Au(111) system using density-functional theory for a wide range of atomic configurations, including on-surface adsorption, pure subsurface adsorption, as well as surface-oxide-like structures. We find that the most energetically favorable configuration at all coverages considered (from 0.06 to 125 ML) is a very thin surface-oxide-like structure with an oxygen coverage of 0.3125 ML, involving quasithreefold-coordinated oxygen atoms, and surface gold atoms which are linearly coordinated to oxygen atoms. This structure is predicted to be stable on the surface up to temperatures of around 420 K at atmospheric pressures, while on-surface chemisorbed oxygen, even at very low coverage, is only metastable. These findings give support to the possibility that such structures may be present and play a role in the heterogeneous oxidation reactions over supported gold nanoparticles and call for further quantitative experimental investigations under controlled conditions that may identify such thin surface-oxide-like structures.

APPENDIX

1. Oxygen molecule

Convergence tests have been carried out for the properties (binding energy, frequency, and bond length) of the oxygen

molecule with regard to the **k**-point sampling, cell size, and energy cutoff. In particular, we used rectangular cells of 9 × 10 × 11, 14 × 15 × 16, and 19 × 20 × 21 bohr^3. Three **k**-point sets were tested, namely, the Γ point, the (0.25, 0.25, 0.25) point, and four special **k** points in the IBZ. Cutoff energies of 22.05, 29.40, and 36.75 Ry (300, 400, and 500 eV) were also considered. The results are given in Table IV. It can be seen that for the smallest supercell, for an energy cutoff of 400 eV and the $\left(\frac{1}{4}, \frac{1}{4}, \frac{1}{4}\right)$ **k** point, the bond length has completely converged, while the frequency and binding energy (per O atom) are converged to within 4 cm^{-1} and 0.004 eV, respectively.

2. Oxygen adsorption

We also tested the convergence of on-surface adsorption of oxygen on Au(111) for the coverages of 0.25, 0.50, 0.75, and 1 ML. For this, we investigated different energy cutoffs as well as the effect of using different SUCs for the same structures, i.e., calculating the 0.25 ML coverage structure with one oxygen atom in the (2×2) SUC and with four oxygen atoms in a (4×4) SUC and the 0.75 ML coverage structure with three oxygen atoms in a (2×2) SUC and with 12 oxygen atoms in a (4×4) SUC. We found that the adsorption energies for the same coverages (0.25 and 0.75 ML) calculated using different SUCs are identical. For the two energy cutoffs, 36.75 and 29.40 Ry (400 and 500 eV), we found that the adsorption energies differed by at most 0.01 eV. The corresponding atomic surface relaxations obtained using the two different energy cutoffs deviated by at most 0.01 Å. Finally, we tested the dependence of the adsorption energy and geometry with respect to

TABLE IV. Convergence tests for the bond length (bl) (in Å), vibrational frequency (ω) (in cm^{-1}), and binding energy of the oxygen molecule (E_b) (in eV) per O atom, with respect to cell size (bohr^3), energy cutoff, and **k** points.

Cell size	Energy cutoff		Γ point	$\left(\frac{1}{4}, \frac{1}{4}, \frac{1}{4}\right)$	$2 \times 2 \times 2$
$9 \times 10 \times 11$	300	bl		1.241	
		ω		1447	
		E_b		3.150	
	400	bl	1.232	1.235	1.235
		ω	1577	1557	1557
		E_b	3.146	3.141	3.142
	500	bl		1.234	
		ω		1558	
		E_b		3.141	
$14 \times 15 \times 16$	400	bl	1.235	1.235	1.235
		ω	1558	1558	1557
		E_b	3.137	3.138	3.138
$19 \times 20 \times 21$	500	bl	1.235	1.235	1.235
		ω	1561	1561	1561
		E_b	3.136	3.137	3.137

k points. Using smaller **k**-point meshes of $10 \times 10 \times 1$ and $8 \times 8 \times 1$ (than the employed $12 \times 12 \times 1$ set) for 1 ML of O on Au(111) resulted in changes in the adsorption energy of 0.02 eV less favorable and 0.006 eV more favorable, respectively, while the O-Au bond lengths changed at most by 0.003 Å.

3. Vibrational contribution to the surface free energy

Vibrational contributions to differences in the Gibbs free energies of extended systems often exhibit some cancellation. However, when there are additional atomic or molecular species which are not present in the reference system [for the present case, the clean Au(111) surface], the situation may be different as there will be no cancellation possible. For the lowest-energy surface-oxide-like structure [Fig. 11(g)], we investigate the contribution due to the adsorbed O atoms. To do this, we calculate the zone-center (Γ-point) normal vibrational modes by diagonalizing the dynamical matrix. We then use the obtained oxygen modes ω_i to evaluate the vibrational and entropic contributions to the Gibbs free energy $\Delta F^{\mathrm{vib}} = E^{\mathrm{vib}} - TS^{\mathrm{vib}}$ as

$$\Delta F^{\mathrm{vib}}(T) = \sum_i \left[\hbar \omega_i \left(\frac{1}{2} + \frac{1}{e^{\beta \hbar \omega_i} - 1} \right) \right.$$
$$\left. - k_B T \left(\frac{\beta \hbar \omega_i}{e^{\beta \hbar \omega_i} - 1} - \ln(1 - e^{-\beta \hbar \omega_i}) \right) \right], \quad (A1)$$

where $\beta = 1/(k_B T)$.[60] We have altogether 15 frequencies since there are five O atoms per cell and each with (x, y, z) modes. Figure 16 shows the resulting curve for $\Delta F^{\mathrm{vib}}(T)$. It can be seen that for a temperature of ~400 K, the contribution is negligible. At 600 K, it gives rise to a stabilization of the surface structure by about 2 meV, and for a temperature of ~250 K, a destabilization by about the same amount is found. Overall, these contributions do not change our qualitative conclusions.
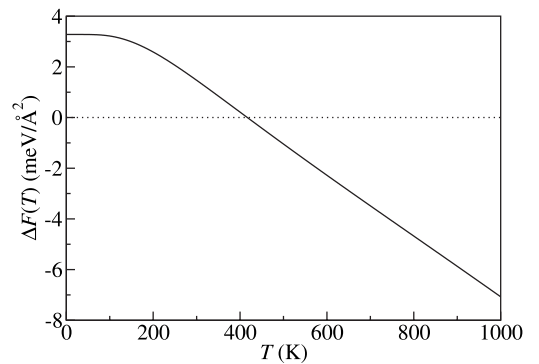
FIG. 16. Vibrational and entropic contributions [cf. Eq. (A1)] to the Gibbs surface free energy for the lowest-energy surface-oxide-like structure [see Fig. 11(g)] due to the oxygen atoms.

[1] G. C. Bond and D. T. Thompson, Catal. Rev. - Sci. Eng. **41**, 319 (1999).

[2] M. Haruta, N. Yamada, T. Kobayashi, and S. Iijima, J. Catal. **115**, 301 (1989).

[3] M. Haruta, Gold Bull. **37**, 27 (2004), and references therein.

[4] R. Meyer, C. Lemire, Sh. K. Shaikhutdinov, and H.-J. Freund, Gold Bull. **37**, 72 (2004), and references therein.

[5] F. Boccuzzi and A. Chiorino, J. Phys. Chem. B **104**, 5414 (2000).

[6] F. Boccuzzi, A. Chiorino, and M. Manzoli, Mater. Sci. Eng., C **15**, 215 (2001).

[7] T. S. Kim, J. D. Stiehl, C. T. Reeves, R. J. Meyer, and C. B. Mullins, J. Am. Chem. Soc. **125**, 2018 (2003).

[8] J. D. Stiehl, T. S. Kim, C. T. Reeves, R. J. Meyer, and C. B. Mullins, J. Phys. Chem. B **108**, 7917 (2004).

[9] L. M. Molina, M. D. Rasmussen, and B. Hammer, J. Chem. Phys. **120**, 7673 (2004).

[10] L. M. Molina and B. Hammer, Appl. Catal., A **291**, 21 (2005).

[11] M. Mavrikakis, P. Stoltze, and J. K. Nørskov, Catal. Lett. **64**, 101 (2000).

[12] D. Ricci, A. Bongiorno, G. Pacchioni, and U. Landman, Phys. Rev. Lett. **97**, 036106 (2006).

[13] M. Yulikov, M. Sterrer, M. Heyde, H.-P. Rust, T. Risse, H.-J. Freund, G. Pacchioni, and A. Scagnelli, Phys. Rev. Lett. **96**, 146804 (2006).

[14] J. G. Wang and B. Hammer, Phys. Rev. Lett. **97**, 136107 (2006).

[15] S. Laursen and S. Linic, Phys. Rev. Lett. **97**, 026101 (2006).

[16] M. A. Chesters and G. A. Somorjai, Surf. Sci. **52**, 21 (1975).

[17] M. E. Schrader, Surf. Sci. **78**, L227 (1978).

[18] N. D. S. Canning, D. Outka, and R. J. Madix, Surf. Sci. **141**, 240 (1984).

[19] P. Legaré, L. Hilaire, M. Sotto, and G. Maire, Surf. Sci. **91**, 175 (1980).

[20] J. J. Pireaux, M. Chtaïb, J. P. Delrue, P. A. Thiry, M. Liehr, and R. Caudano, Surf. Sci. **141**, 211 (1984).

[21] J. J. Pireaux, M. Liehr, P. A. Thiry, J. P. Delrue, and R. Caudano, Surf. Sci. **141**, 221 (1984).

[22] D. H. Parker and B. E. Koel, J. Vac. Sci. Technol. A **8**, 2585 (1990); M. A. Lazaga, D. T. Wickham, D. H. Parker, G. N. Kastanas, and B. E. Koel, Am. Chem. Soc. Symp. Ser. **523**, 90 (1993).

[23] A. Krozer and M. Rodah, J. Vac. Sci. Technol. A **15**, 1704 (1997).

[24] D. E. King, J. Vac. Sci. Technol. A **13**, 1247 (1995).

[25] F. Cotton and G. Wilkinson, *Inorganic Chemistry*, 3rd ed. (Wiley, New York, 1972), p. 994.

[26] N. Saliba, D. H. Parker, and B. E. Koel, Surf. Sci. **410**, 270 (1998).

[27] K. A. Davis and D. W. Goodman, J. Phys. Chem. B **104**, 8557 (2000).

[28] J. Cao, N. Wu, S. Qi, K. Feng, and M. S. Zei, Chin. Phys. Lett. **6**, 92 (1989).

[29] J. Chevrier, L. Huang, P. Zeppenfeld, and G. Comsa, Surf. Sci. **355**, 1 (1996).

[30] L. Huang, J. Chevrier, P. Zeppenfeld, and G. Comsa, Appl. Phys. Lett. **66**, 935 (1995).

[31] L. Huang, J. Chevrier, P. Zeppenfeld, and G. Comsa, Appl. Phys. Lett. **66**, 935 (1995); L. Huang, P. Zeppenfeld, J. Chevrier, and G. Comsa, Surf. Sci. **352**, 285 (1996); J. Chevrier, L. Huang, P. Zeppenfeld, and G. Comsa, *ibid.* **355**, 1 (1996); Y. Uchida, X. Bao, K. Weiss, and R. Schlögl, *ibid.* **401**, 469 (1998); L. Ortega, L. Huang, J. Chevrier, P. Zeppenfeld, J. M. Gay, F. Rieutord, and G. Comsa, Surf. Rev. Lett. **4**, 1315 (1997).

[32] Y. Uchida, X. Bao, K. Weiss, and R. Schlögl, Surf. Sci. **401**, 469 (1998).

[33] X. Bao, J. V. Barth, G. Lehmpfuhl, R. Schuster, Y. Uchida, R. Schlögl, and G. Ertl, Surf. Sci. **284**, 14 (1993).

[34] H. Schubert, U. Tegtmeyer, D. Herein, X. Bao, M. Muhler, and R. Schlögl, Catal. Lett. **33**, 305 (1995).

[35] S. M. McClure, T. S. Kim, J. D. Stiehl, P. L. Tanaka, and C. B. Mullins, J. Phys. Chem. B **108**, 17952 (2004).

[36] X. Y. Deng, B. K. Min, A. Guloy, and C. M. Friend, J. Am. Chem. Soc. **127**, 9267 (2005).

[37] B. K. Min, X. Deng, D. Pinnaduwage, R. Shalek, and C. M. Friend, Phys. Rev. B **72**, 121410(R) (2005).

[38] Z. P. Liu, P. Hu, and A. Alavi, J. Am. Chem. Soc. **124**, 14770 (2002).

[39] Y. Xu and M. Mavrikakis, J. Phys. Chem. B **107**, 9298 (2003).

[40] K. Reuter, C. Stampfl, M. V. Ganduglia-Pirovano, and M. Scheffler, Chem. Phys. Lett. **352**, 311 (2002).

[41] K. Reuter, M. V. Ganduglia-Pirovano, C. Stampfl, and M. Scheffler, Phys. Rev. B **65**, 165403 (2002).

[42] J. Gustafson, A. Mikkelsen, M. Borg, E. Lundgren, L. Köhler, G. Kresse, M. Schmid, P. Varga, J. Yuhara, X. Torrelles, C. Quirós, and J. N. Andersen, Phys. Rev. Lett. **92**, 126102 (2004).

[43] M. V. Ganduglia-Pirovano and M. Scheffler, Phys. Rev. B **59**, 15533 (1999).

[44] H. Zhang, A. Soon, B. Delley, and C. Stampfl (unpublished).

[45] M. Todorova, K. Reuter, and M. Scheffler, Phys. Rev. B **71**, 195403 (2005); J. Phys. Chem. B **108**, 14477 (2004).

[46] W. X. Li, C. Stampfl, and M. Scheffler, Phys. Rev. Lett. **90**, 256102 (2003).

[47] A. Michaelides, K. Reuter, and M. Scheffler, J. Vac. Sci. Technol. A **23**, 1487 (2005).

[48] W. X. Li, C. Stampfl, and M. Scheffler, Phys. Rev. B **67**, 045408 (2003).

[49] A. Soon, M. Todorova, B. Delley, and C. Stampfl, Phys. Rev. B **73**, 165424 (2006).

[50] M. Todorova, W. X. Li, M. V. Ganduglia-Pirovano, C. Stampfl, K. Reuter, and M. Scheffler, Phys. Rev. Lett. **89**, 096103 (2002).

[51] G. Kresse and J. Hafner, Phys. Rev. B **47**, 558 (1993); **49**, 14251 (1994).

[52] G. Kresse and J. Furthmüller, Comput. Mater. Sci. **6**, 15 (1996).

[53] G. Kresse and J. Furthmüller, Phys. Rev. B **54**, 11169 (1996).

[54] G. Kresse and D. Joubert, Phys. Rev. B **59**, 1758 (1999).

[55] P. E. Blöchl, Phys. Rev. B **50**, 17953 (1994).

[56] J. P. Perdew, J. A. Chevary, S. H. Vosko, K. A. Jackson, M. R. Pederson, D. J. Singh, and C. Fiolhais, Phys. Rev. B **46**, 6671 (1992).

[57] J. Neugebauer and M. Scheffler, Phys. Rev. B **46**, 16067 (1992).

[58] M. Scheffler and C. Stampfl, in *Electronic Structure*, edited by K. Horn and M. Scheffler, Handbook of Surface Science Vol. 2 (Elsevier, Amsterdam, 1999).

[59] W. X. Li, C. Stampfl, and M. Scheffler, Phys. Rev. B **65**, 075407 (2002).

[60] K. Reuter, M. V. Ganduglia-Pirovano, C. Stampfl, and M. Scheffler, Phys. Rev. B **65**, 165403 (2002).

[61] C. M. Weinert and M. Scheffler, Mater. Sci. Forum **10-12**, 25 (1986).

[62] M. Scheffler, in *Physics of Solid Surfaces-1987*, edited by J. Koukal (Elsevier, Amsterdam 1988), p. 115; M. Scheffler and J.

Dabrowski, Philos. Mag. A **58**, 107 (1988).

[63] E. Kaxiras, Y. Bar-Yam, J. D. Joannopoulos, and K. C. Pandey, Phys. Rev. B **35**, 9625 (1987).

[64] G.-X. Qian, R. M. Martin, and D. J. Chadi, Phys. Rev. B **38**, 7649 (1988).

[65] X. G. Wang, W. Weiss, Sh. K. Shaikhutdinov, M. Ritter, M. Petersen, F. Wagner, R. Schlögl, and M. Scheffler, Phys. Rev. Lett. **81**, 1038 (1998).

[66] K. Reuter and M. Scheffler, Phys. Rev. B **65**, 035406 (2001).

[67] D. R. Stull and H. Prophet, *JANAF Thermochemical Tables*, 2nd ed. (U.S. National Bureau of Standards, Washington, DC, 1971).

[68] M. Garst, P. Wölfle, L. Borda, J. von Delft, and L. Glazman, Phys. Rev. B **72**, 205125 (2005).

[69] *The Oxide Handbook*, edited by G. V. Samsonov (IFI/Plenum, New York, 1973).

[70] *Handbook of Chemistry and Physics* Vol. 69, edited by R. C. Weast, M. J. Astle, and W. H. Beyer (CRC, Boca Raton, FL, 1989).

[71] O. Kubaschewski, C. B. Alcock, and P. J. Spencer, *Materials Thermochemistry* (Pergamon, Oxford, 1993).

[72] C. Kittel, *Introduction to Solid State Physics* (Wiley, New York, 1996).

[73] B. D. Yu and M. Scheffler, Phys. Rev. B **56**, R15569 (1997).

[74] L. L. Wang and H. P. Cheng, Phys. Rev. B **69**, 165417 (2004).

[75] G. V. Hansson and S. A. Flodstrom, Phys. Rev. B **18**, 1572 (1978).

[76] K. P. Huber and G. Herzberg, *Molecular Spectra and Molecular Structure IV: Constants of Diatomic Molecules* (Van Nostrand Reinhold, New York, 1979).

[77] J. P. Perdew, K. Burke, and M. Ernzerhof, Phys. Rev. Lett. **77**, 3865 (1996).

[78] A. Eichler, F. Mittendorfer, and J. Hafner, Phys. Rev. B **62**, 4744 (2000).

[79] Y. Xu and M. Mavrikais, Surf. Sci. **494**, 131 (2001).

[80] Y. Xu and M. Mavrikais, J. Chem. Phys. **116**, 10846 (2002).

[81] C. Stampfl, S. Schwegmann, H. Over, M. Scheffler, and G. Ertl, Phys. Rev. Lett. **77**, 3371 (1996).

[82] C. Stampfl and M. Scheffler, Phys. Rev. B **54**, 2868 (1996).

[83] G. Boisvert, L. J. Lewis, M. J. Puska, and R. M. Nieminen, Phys. Rev. B **52**, 9078 (1995).

[84] J. Schnadt, A. Michaelides, J. Knudsen, R. T. Vang, K. Reuter, E. Laegsgaard, M. Scheffler, and F. Besenbacher, Phys. Rev. Lett. **96**, 146101 (2006).

[85] M. Schmid, A. Reicho, A. Stierle, I. Costina, J. Klikovits, P. Kostelnik, O. Doubay, G. Kresse, J. Gustafson, E. Lundgren, J. N. Anderson, H. Dosch, and P. Varga, Phys. Rev. Lett. **96**, 146102 (2006).